frontiers | Frontiers in Astronomy and Space Sciences

TYPE Original Research
PUBLISHED 03 August 2023
DOI 10.3389/fspas.2023.1191294

OPEN ACCESS

EDITED BY
Mario J. P. F. G. Monteiro,
University of Porto, Portugal

REVIEWED BY
João José Graça Lima,
Universidade do Porto, Portugal
David Barnes,
Science and Technology Facilities Council, United Kingdom

*CORRESPONDENCE
Tatiana Niembro,
tniembro@cfa.harvard.edu

RECEIVED 21 March 2023
ACCEPTED 02 June 2023
PUBLISHED 03 August 2023

CITATION
Niembro T, Seaton DB, Hess P, Berghmans D, Andretta V, Reeves KK, Riley P, Stevens ML, Landini F, Sasso C, Verbeeck C, Susino R and Uslenghi M (2023), A prominence eruption from the Sun to the Parker Solar Probe with multi-spacecraft observations. *Front. Astron. Space Sci.* 10:1191294. doi: 10.3389/fspas.2023.1191294

A prominence eruption from the Sun to the Parker Solar Probe with multi-spacecraft observations

Tatiana Niembro[1]*, Daniel B. Seaton[2], Phillip Hess[3], David Berghmans[4], Vincenzo Andretta[5], Katharine K. Reeves[1], Pete Riley[6], Michael L. Stevens[1], Federico Landini[7], Clementina Sasso[5], Cis Verbeeck[4], Roberto Susino[7] and Michela Uslenghi[8]

[1]Center for Astrophysics, Harvard & Smithsonian, Cambridge, MA, United States, [2]Southwest Research Institute, Boulder, CO, United States, [3]U.S. Naval Research Laboratory, Washington, DC, United States, [4]Solar-Terrestrial Centre of Excellence—SIDC, Royal Observatory of Belgium, Brussels, Belgium, [5]INAF—Osservatorio Astronomico di Capodimonte, Naples, Italy, [6]Predictive Science Inc., San Diego, CA, United States, [7]Istituto di Astrofisica Spaziale e Fisica Cosmica, Osservatorio Astrofisico di Torino, Pino Torinese, Italy, [8]INAF—Istituto di Astrofisica Spaziale e Fisica Cosmica, Milan, Italy

In the early hours of 2021 April 25, the Solar Probe Cup on board Parker Solar Probe registered the passage of a solar wind structure characterized by a clear and constant He^{2+}/H^{+} density ratio above 6% during three hours. The He^{2+} contribution remained present but fainting and intermittent within a twelve-hour window. Solar Orbiter and Parker Solar Probe were in nearly perfect quadrature, allowing for optimal observing configuration in which the material impacting the Parker Solar Probe was in the Solar Orbiter plane of the sky and visible off the limb. In this work, we report the journey of the helium-enriched plasma structure from the Sun to the Parker Solar Probe by combining multi-spacecraft remote-sensing and *in situ* measurements. We identify an erupting prominence as the likely source, behind the Sun relative to the Earth, but visible to multiple instruments on both the Solar-Terrestrial Relations Observatory-A and Solar Orbiter. The associated CME was also observed by coronagraphs and heliospheric imagers from both spacecrafts before reaching the Parker Solar Probe at 46 $R_{\odot}$, 8 h after the spacecraft registered a crossing of the heliospheric current sheet. Except for extraordinary helium enhancement, the CME showed ordinary plasma signatures and a complex magnetic field with an overall strength enhancement. The images from the Wide-field Imager for Solar Probe (WISPR) aboard Parker Solar Probe show a structure entering the field of view a few hours before the *in situ* crossing, followed by repetitive transient structures that may be the result of flying through the CME body. We believe this to be the first example of a CME being imaged by WISPR directly before and during being detected *in situ*. This study highlights the potential of combining the Parker Solar Probe *in situ* measurements in the inner heliosphere with simultaneous remote-sensing observations in (near) quadrature from other spacecrafts.

KEYWORDS

prominence, coronal mass ejection, space weather, multi-spacecraft observations, Parker Solar Probe

1 Introduction

Coronal mass ejections (CMEs) are sudden releases of large amounts of plasma dragging magnetic fields throughout the heliosphere (Webb and Howard, 2012). CMEs have been imaged in remote-sensing data since the 1970s, with missions such as OSO-7 (Tousey et al., 1973), Skylab (MacQueen et al., 1974), the Solar Maximum Mission (MacQueen et al., 1980), and P78-1 (Solwind; Sheeley et al., 1980).

Shortly after the first observation, a relationship was discovered between CMEs at the Sun, and *in situ* signatures recorded near the Earth (Burlaga et al., 1982) further strengthened in the following years (Richardson et al., 2000). The remote-sensing observations were improved with the continuous, near-Earth imaging of the Large Angle and Spectrometric COronagraph Experiment (LASCO, Brueckner et al., 1995) aboard the SOlar and Heliospheric Observatory (SOHO, Domingo et al., 1995), beginning in 1996 and still operating today. Moreover, since 2006, after the launch of the Solar TErrestrial RElations Observatory (STEREO, Kaiser, 2005), multiple viewpoints and imaging from the solar surface to beyond 1 au are obtained with the Sun Earth Connection Coronal and Heliospheric Investigation instrument suite (SECCHI, Howard et al., 2008).

This improved observational coverage allowed a direct link between the imaging data and *in situ* data (Rouillard, 2011; DeForest et al., 2013), followed by statistical studies comparing properties of CMEs throughout the heliosphere to the *in situ* properties (Hess and Zhang, 2017; Wood et al., 2017) of their counterparts, the interplanetary coronal mass ejections (ICMEs). From a comprehensive analysis of 310 ICMEs, Zurbuchen et al. (2016) found that not only ICMEs exhibit systematic element abundance enhancements compared to quasi-stationary solar wind but also that the *in situ* composition measurements provide a unique way to determine the location and dynamics of their source region. Furthermore, it was found that more than 70% of CMEs are associated with prominence eruptions (Munro et al., 1979; Gopalswamy et al., 2003), which are related to the settlement of cool and dense plasma in the highly sheared, mainly horizontal, magnetic field above polarity-inversion lines (Priest et al., 1989; Gibson, 2018). Moreover, inside ICMEs, the composition has been found to be elevated in He^{2+}/H^{+} (Borovsky, 2008; Yermolaev et al., 2020) particularly with larger values when the ICMEs are related to prominences (Hirshberg et al., 1972; Borrini et al., 1982; Lepri and Rivera, 2021).

Prominence eruptions are routinely observed, near the Sun, with visible (e.g., Hα) and extreme ultraviolet (EUV) telescopes, in the middle corona with visible light coronagraphs and with heliospheric imagers at larger distances from the Sun (a review on prominence observations can be found in Parenti, 2014, and references *therein*). In favorable circumstances, these remote-sensing observations may be supplemented by *in situ* measurements, which provide highly localized information about the speed, composition, and magnetic field.

While propagating from the Sun into the heliosphere, prominences and associated CMEs must be observed in widely disparate domains as no single instrument can provide an overview of their evolution (Thernisien et al., 2009; Luhmann et al., 2020). For the most part, gaps between these measurements and the challenges of processing data in a unified way have inhibited complete analyses of eruption initiation and propagation to *in situ* instruments.

In contrast, one example of this kind of study that *does* achieve the rare unification of observations that span from the Sun to the heliosphere is described in a series of papers by Howard and DeForest (2012) and DeForest et al. (2013), using data from STEREO-A, the Advance Composition Explorer (ACE, Stone et al., 1998), the Wind spacecraft (Ogilvie and Desch, 1997), and extensive image processing to track a small CME from its genesis at the Sun through the heliosphere to Earth.

More recently, studies have demonstrated the feasibility of closing some important observational gaps in the early evolution of erupting prominences using extended EUV observations. Reva et al. (2016) used the TESIS instrument assembly on the Russian CORONAS-PHOTON mission, along with images from LASCO, to observe the onset and early evolution of an erupting prominence, producing a complete trajectory from initiation to about 25 $R_{\odot}$. Seaton et al. (2021) used a special campaign of the GOES Solar Ultraviolet Imager to track several small eruptions continuously from the solar surface to heights that are well-observed by coronagraphs. Other studies have leveraged the large field of view and off-pointing capabilities of the SWAP EUV imager on PROBA2 to characterize the early evolution of eruptions (O'Hara et al., 2019) and, when combined with STEREO-A observations, to develop three-dimensional understanding of erupting features (Mierla et al., 2013).

The advent of the Parker Solar Probe (PSP, Fox et al., 2016) and Solar Orbiter (SolO, Müller et al., 2020) missions has provided a new opportunity to study the origins and evolution of eruptions as they propagate from the Sun into the heliosphere. With a highly elliptical orbit that, using a series of gravity assists from Venus, will continue to get closer to the Sun, PSP enables an unprecedented ability to observe at heliospheric distances as close to the Sun as 0.04 au (less than 9 $R_{\odot}$). While not getting as close to the Sun as PSP, SolO still takes science observations down to 0.28 au (60 $R_{\odot}$) and further improves observational coverage with remote-sensing capabilities extending from the EUV to visible light, including coronagraphy and, at a later stage of the mission, by leaving the ecliptic plane.

Given the combined ability to observe both near the Sun and off of the Sun–Earth line, these spacecrafts significantly extend our ability to track eruptions continuously, with multiple perspectives, and the capability to directly sample localized plasma and magnetic conditions within an eruption and, when combined with additional observations, three-dimensional characterization of these features.

Unlike the past 1 au missions, PSP and SolO, due to their rapid changes in radial distance from the Sun, are not intended to take consistent data at regular intervals but are instead designed to focus science observations at specific periods and locations. Given the need to inform the *in situ* observations at one satellite with the context of remote-sensing observations at another, exploiting the uniquely advantageous orbital configurations is vital to achieving deep understanding, significantly augmenting the science results that could be achieved by any individual mission (Velli et al., 2020).

A favorable configuration occurred in late 2021 April, while PSP was approaching its eighth perihelion and was in near quadrature with SolO. Rodriguez et al. (2023) reported in detail an eruptive event that happened on 2021 April 22. With multiple independent lines of evidence (from different instruments and spacecraft),

they showed, for the first time, the direct connection between the eruption and continuous magnetic reconnection and heating processes. The related ICME, which arrived on the Earth late on 2021 April 24, causing a minor geomagnetic storm, highlights the importance to establish a connection between solar eruptions observed in the solar corona and their *in situ* signatures measured by spacecraft in interplanetary space.

Two days later, during the late hours of 2021 April 23, another unrelated eruption event took place, reaching PSP in the early hours of 2021 April 25. In this investigation, we identify the eruption of prominence material at the surface of the Sun as the source of a helium-enriched plasma structure measured *in situ* by the PSP spacecraft. We use multi-spacecraft remote-sensing observations (STEREO-A and SolO) to track the propagation of the associated CME from the Sun to the PSP location.

This work is organized as follows. In Section 2, we describe the models, locations, and datasets of the different spacecraft used to track the CME from the Sun to PSP. In Section 3, we present the PSP *in situ* observations and how we use them to predict solar wind conditions at 10–20 $R_\odot$. Then, we present an overview of the remote-sensing observations (Section 4): from the EUV images (Section 4.1), coronagraphs (Section 4.2), and heliospheric images (Section 4.3). The results of the reconstruction using the Graduated Cylindrical Shell model (GCS Thernisien et al., 2006; Thernisien et al., 2009) are shown in Section 4.4. Finally, we summarize, discuss our results in a height–time plot (distances between 1.5 and 20 $R_\odot$) combining all observations, and present our conclusions in Section 5.

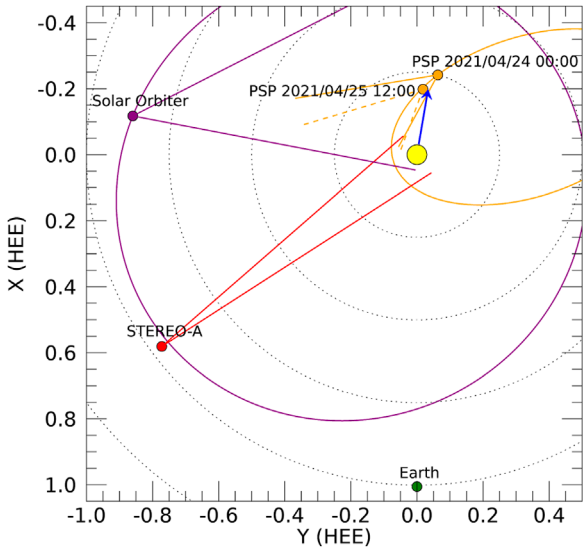

FIGURE 1
Location of Earth, SolO, and STEREO-A spacecraft when the CME impacted PSP on 2021 April 25 at 01:00 UT given in Heliocentric Earth Ecliptic (HEE) coordinates. The *blue* arrow represents the approximate propagation direction of the CME as determined from a forward modeling reconstruction of the eruption. The PSP and STEREO-A orbits are shown in *orange* and *purple* solid circles, respectively. Two PSP locations are shown, representing the inbound trajectory of the spacecraft. PSP and SolO were in nearly perfect quadrature during the event, allowing the observation of the eruption from the SolO plane of the sky. The lines on the plot show the cumulative fields of view from the remote-sensing instruments of each spacecraft used in this study. The changing field of view for WISPR is highlighted by the difference between the solid (earlier) and dashed (later) lines. The position of SDO can be assumed to be that of the Earth.

2 Data, spacecraft location, and models

To study the full evolution of the event, we combine the *in situ* detectors on board Parker Solar Probe (PSP, Fox et al., 2016), including the plasma parameter measurements from the Solar Wind Electrons Alphas and Protons (SWEAP, Kasper et al., 2016) and the Electromagnetic Fields Investigation (FIELDS, Bale et al., 2016) instruments, with remote-sensing observations from the Solar TErrestrial RElations Observatory (STEREO, Kaiser, 2005), Solar Orbiter (SolO, Müller et al., 2020), and PSP. Due to the location of the prominence on the far side of the Sun from the Earth's perspective (see Figure 1), there were no obvious signatures in any Earth-orbiting *in situ* or remote-sensing observatories.

On PSP, the *in situ* plasma conditions are obtained from the data registered by three electrostatic analyzers, called the Solar Probe ANalyzers (SPAN, Whittlesey et al., 2020), and the Solar Probe Cup (SPC, Case et al., 2020), which are part of SWEAP suite, while the magnetic field measurements are from FIELDS instrument. On SolO, the plasma is measured by the Solar Wind Analyzer (SWA, Owen et al., 2020) and the magnetic fields with the magnetometer (MAG, Horbury et al., 2020).

For remote sensing, SolO carries the Extreme Ultraviolet Imager (EUI, Rochus et al., 2020), the Metis coronagraph (Antonucci et al., 2020), and the SolO Heliospheric Imager (SoloHI, Howard et al., 2020). EUI includes the Full Sun Imager (FSI), a wide field of view EUV imager with 174 and 304 Å channels which overlaps with the fields of view of Metis, that images the corona in the Visible and Ly-α. PSP, in addition to extensive *in situ* instrumentation, and carries its own Wide-field Imager for Solar Probe (WISPR, Vourlidas et al., 2016). STEREO images are obtained with the Sun-Earth Connection Coronal and Heliospheric Investigation instrument suite (SECCHI, Howard et al., 2008) consisting of five telescopes: an EUV imager (EUVI), two white light coronagraphs (COR1 and COR2), and two wide-field imagers (HI-1 and HI-2).

To image the prominence near the Sun, in the inner and middle corona, we use FSI from SolO and SECCHI from STEREO-A spacecraft. FSI was operating alternatively in its 174 and 304 Å channels, resulting in over eight images per hour of each type (Mampaey et al., 2022). SolO was at 0.87 au distance from the Sun, resulting in an FSI field of view of 12.4 $R_\odot$.

In the middle and outer corona, we utilize the COR2 and Metis coronagraphs. The Metis white light (WL) and Lyman-α channel observations were obtained during a synoptic program, with a cadence of one dataset per hour. Each dataset consists of four polarized (WL) images, which, combined together, produce one (pB) image and three UV images. The acquired data were processed and calibrated following the procedure described in Romoli et al. (2021) and subsequently updated by Andretta et al. (2021). Small variations of the baseline level of data in the UV channel were corrected with a procedure devised and later implemented in the standard data processing pipeline.

TABLE 1 Positions (longitude, latitude, and radial distance) in HEE coordinates of PSP, SolO, and STEREO-A on 2021 April 24 at 00:00 UT. The values in parentheses are PSP position on 2021 April 25 at 00:00 UT, 1 hour before the arrival detection of the structure at PSP. The other missions remained quasi-stationary throughout the period. The remote-sensing instruments used from each spacecraft have been listed along with their observed physical quantities (white light (WL), extreme ultraviolet (EUV), and Lyman–α radiation) and field of views (FOVs), respectively. The FOVs listed are approximations of the radial heights of the angular field of view at the radial distance of the respective individual spacecraft.

Spacecraft	Instrument	Lon (°)	Lat (°)	R ($R_\odot$)	Observation(s)	FOV ($R_\odot$)
Parker Solar Probe	WISPR-I	165.4(171.1)	−2.9(−2.6)	53.8(46.6)	WL	13–45(11–38)
	WISPR-O	"	"	"	WL	41–87(36–76)
STEREO-A	SECCHI/EUVI	307.0	−0.1	207.8	EUV	1–1.7
	SECCHI/COR2	"	"	"	WL	2.5–15
SolO	EUI/FSI	262.2	4.9	187.1	EUV	1–6
	Metis	"	"	"	WL/Lyman-α	5–10
	SoloHI	"	"	"	WL	16–130

Imaging at even greater heights is provided by SoloHI and WISPR. SoloHI observes off the east limb of the Sun with a 40° field of view, centered near 25° from the center of the solar disk. SoloHI consists of four separate 2k×2k APS detectors, arranged in a square pattern and sharing a single optical system for a total 4k×4k field of view. The boundaries between these tiles form a visible, stable cross-pattern in the images when the four tiles are correctly assembled into a single mosaic. WISPR consists of two 2k×2k APS detectors. The WISPR-Inner telescope (WISPR-I) has a 40° field of view, centered approximately 13.5° off the western limb of the Sun, relative to the spacecraft. The WISPR-Outer telescope (WISPR-O) has a 60° field of view centered at approximately 73°.

The locations of Earth, PSP, STEREO-A, and SolO are shown in Figure 1 in the Heliocentric Earth Ecliptic (HEE) coordinate system. PSP and SolO orbits are shown in *orange* and *purple* solid lines, respectively. PSP and SolO were in nearly perfect quadrature when the CME was launched to space from the Sun (its direction is marked with a *blue* arrow in the figure), allowing us the remote-sensing observation of the eruption from SolO's point of view. In Table 1, we summarize the radial distance (R), longitude (lon), and latitude (lat) of all spacecraft. In both Figure 1 and Table 1, the locations of PSP are given for both the approximate onset time of the prominence eruption as well as for 24 h later, when the *in situ* signatures are first observed. In this time span, PSP moves 5.7° in longitude and 7.2 $R_\odot$ toward the Sun.

We model the background magnetic field using the Magnetohydrodynamic (MHD) Algorithm outside a Sphere (MAS) model from Predictive Science Inc. (PSI). We use the semi-empirical thermodynamic approach described in Riley et al. (2021), which includes conductive and radiative losses, and an empirical term for the coronal heating term (see Lionello et al., 2001; 2009; Reeves et al., 2010, for details involved in solving the MHD equations). The model consists of coronal solution (1–30 $R_\odot$) and heliospheric solution (30 $R_\odot$—1 au), with the heliospheric solution being driven by the results of the coronal solution. The boundary conditions for the coronal solution are derived from the Helioseismic and Magnetic Imager (HMI Schou et al., 2012) aboard Solar Dynamics Observatory (SDO Pesnell et al., 2012), and the boundary conditions for the heliospheric solution are based on the Distance from the Coronal Hole Boundary (DCHB) method (Riley et al., 2001; 2015). This model has been found to have very good agreement with magnetic field measurements taken *in situ* at the Earth, STEREO-A, and PSP for the first four PSP perihelia (Riley et al., 2021). Figure 2 shows the magnetic field obtained from the model and its relationship to the Sun and the location of PSP during the eruption.

In order to model the kinematics of the CME, we use the Graduated Cylindrical Shell model (GCS Thernisien et al., 2006; Thernisien et al., 2009), which is an empirical geometric model used to represent the flux-rope configuration of CMEs. This model was used to reconstruct many CMEs from LASCO and SECCHI data (e.g., Hess and Zhang, 2017; Kilpua et al., 2019; Zhao et al., 2019; Scolini et al., 2020; Palmerio et al., 2021; Nieves-Chinchilla et al., 2022). The same approach can be adapted to include WISPR and SoloHI data while still including the older datasets (Braga et al., 2022).

To reconstruct the solar wind conditions from PSP data (speed and density) back to 10–20 $R_\odot$, we solve Bernoulli's equation (Landau and Lifshitz, 1987) assuming the adiabatic expansion of a polytropic flow and neglecting the contribution of gravity force. Backward reconstruction methods have been extensively used (Parker, 1958; Weber and Davis, 1967; Tasnim et al., 2018; Biondo et al., 2021) with their limitations extensively discussed (Schatten, 1971; Pizzo, 1981; Ness and Burlaga, 2001).

3 The *in situ* observation of a helium-enriched plasma structure

In Figure 3, from *top* to *bottom*, we show the 15-min time series of the PSP *in situ* measurements of (*first* panel) the normalized differential energy flux versus azimuth angle $SPAN-\phi$ computed from SPAN instrument (Livi et al., 2022); (*second* panel) the PSP distance to the Sun (R, in *black*) with both flow angles $SPC-\theta$ (in *peach*) and $SPC-\phi$ (in *teal*) measured from SPC (Case et al., 2020)[1]; (*third* panel) the magnitude of the proton speed by both SPC

1 SWEAP instrument suite measures the particles of the solar wind, including the direction of the flows. SPC is optimized for flows perpendicular to the PSP heat shield, while SPAN is for flows at wider angles

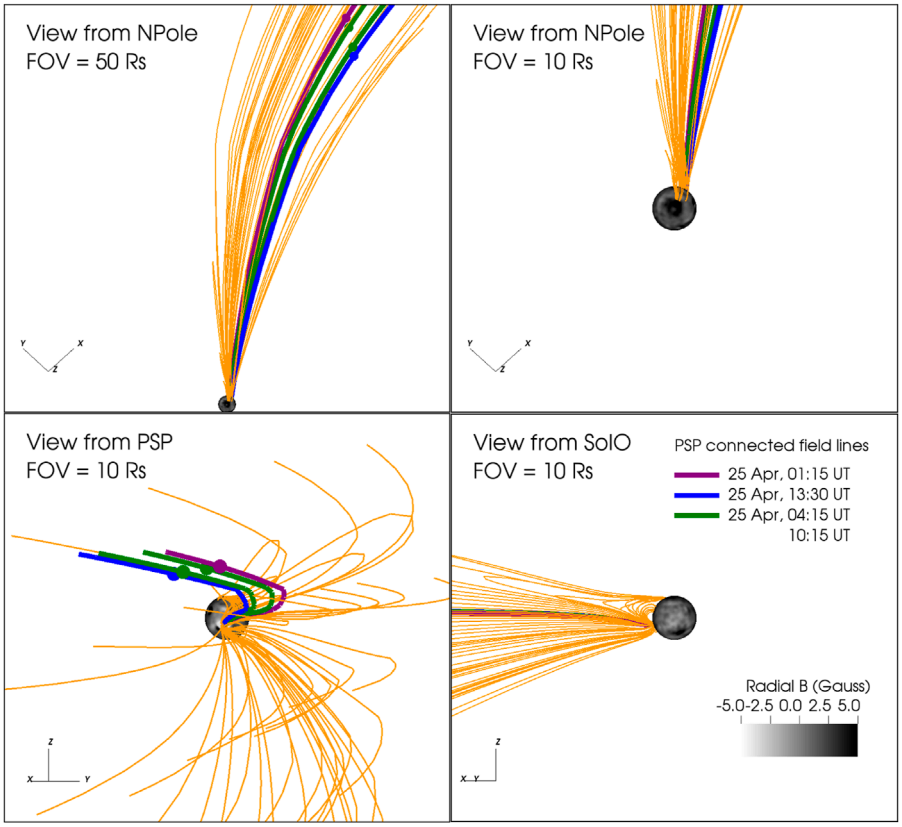

FIGURE 2
Different views (NPole—solar North Pole, PSP, SolO) of model field lines using the PSI/MAS model. Arbitrary magnetic field lines are drawn in *orange* showing open and close magnetic field configurations near the surface of the Sun. We mapped and colored four magnetic field lines connecting the surface of the Sun with PSP (colored *dot* symbols). The *purple* field line is related to the arrival time of the first structure at PSP reaching a maximum speed of 420 km s^{-1}. The two *green* field lines delimit a flow region of constant speed (300 km s^{-1}). The *blue* field line corresponds to a second structure moving at 350 km s^{-1}.

(SPC-$|V|$ in *black*) and SPAN (SPAN-$|V|$ in *gray*) and the magnetic field strength ($|B|$, shown in *navy*) overplot. In the *fourth* panel, we show the radial (B_R, in *blue*), tangential (B_T, in *green*), and normal (B_N, in *red*) components (measured by FIELDS). Then, in the *fifth* panel, the electron pitch angle (PA) for an energy of 314.45 eV with the color scale represents the logarithm of the energy flux vs. PA (from SPAN instrument, Whittlesey et al., 2020). In the *sixth* panel, we show the velocity distribution functions (VDFs) measured by SPC. Then, we present the SPC-β parameter and proton temperature (SPC-T) in the *seventh* panel while SPC-N and SPAN-N densities in the *eighth* panel.

For this period, the majority of the solar wind flow was out of the SPAN field of view ($SPAN - \phi > 160°$, *top* panel) resulting in large and systematic underestimates in the proton density, SPAN-N (*bottom* in Figure 3), from that instrument. The solar wind is fully within the SPC sensor field of view; however, the flow SPC-ϕ direction (*second* panel) is only roughly estimated due to the *crosstalk* anomaly described in the SPC data quality flags. For this analysis, we approximate that $|V| \sim |V_R|$, which is roughly consistent with both sets of observations. We note that the SPAN spectrogram, capturing the tail of the proton distribution, does not show significant signs of flow deflection for at least the first half of the period.

PSP crossed over the heliospheric current sheet (HCS) on 2021 April 24 16:15 UT. Before this time, the magnetic field components and plasma parameters show quiet solar wind conditions, the flow was propagating at a speed between 230 and 260 km s^{-1} and positive B_R value. The electron pitch angle corroborates the change of magnetic field sector which we marked with a *black* vertical dash line. After the HCS crossing, the spacecraft passed through a high-density region (reaching a maximum value of 692 cm^{-3}) traveling at a very low speed of 250 km s^{-1}.

The structure of interest arrived at the spacecraft on 2021 April 25 at 01:15 UT (marked with *purple* dashed vertical line) with no shock signatures and characterized by SPC-N = 214 cm^{-3}, SPC-T = 96,423 K, β = 0.38, and $|B|$ = 73 nT. The low density, beta parameter, and temperature values have been found as characteristic *in situ* signatures of magnetic clouds (Zurbuchen and Richardson, 2006). Moreover, in several investigations, it has been suggested that magnetic clouds are related to the eruption of prominence material (Bothmer and Schwenn, 1994; Burlaga et al., 1998; Wang et al., 2018).